Debris Mitigation and Atmospheric Deorbiting Analysis for Lunar L2 NRHO Departing Spacecraft

74th International Astronautical Congress (IAC), Baku, Azerbaijan, 2-6 October 2023.

IAC-23-78063

Debris Mitigation and Atmospheric Deorbiting Analysis for Lunar L2 NRHO Departing Spacecraft

Carmela Marika Accettura[a]*, Luigi Mascolo[b], Manuela Battipede[c]

[a] *Department of Mechanical and Aerospace Engineering, Politecnico di Torino, Corso Duca degli Abruzzi 24, Turin, Italy,* carmelamarika.accettura@studenti.polito.it
[b] *Department of Mechanical and Aerospace Engineering, Politecnico di Torino, Corso Duca degli Abruzzi 24, Turin, Italy,* luigi.mascolo@polito.it
[c] *Department of Mechanical and Aerospace Engineering, Politecnico di Torino, Corso Duca degli Abruzzi 24, Turin, Italy,* manuela.battipede@polito.it
* Corresponding Author

Abstract

In recent decades, there has been a desire to establish permanent human settlements on the Moon, leading to the proposal and development of the Lunar Orbital Platform-Gateway (LOP-G), the first cislunar orbital laboratory, stationed on a L2 Near Rectilinear Halo Orbit (NRHO). This project will result in a significant increase in the number of spacecrafts in the cislunar space in the near future. To comply with new space debris regulations, e.g., the recent FCC 5-year deorbit rule to avoid the pollution of cislunar space, proper disposal of spacecraft in such region of space is necessary and advisable. However, most past missions have been directed to impact the lunar surface, which may not be a sustainable long-term solution. Therefore, this paper aims to propose an alternative strategy for debris mitigation of satellites, which involves transferring them from NRHO to Low-Earth Orbits (LEOs) and performing a controlled re-entry. The departure location is the reference LOP-G orbit, designed around the Earth-Moon Lagrangian Point L2 (EML2) as a southern NRHO with 9:2 synodic lunar resonance, computed using a Circular Restricted Three-Body dynamic model. The complete family of Halo Orbits, starting from the Lyapunov planar bifurcation up to the 9:2 NRHO, is obtained via Differential Corrector (DC) strategies and single-shooting methods. Then, through the implementation of a genetic algorithm as an optimisation method, the instability of the NRHO orbit is exploited to perform a lunar fly-by and conclude the re-entry to LEO orbit with a second impulse. The analysis is completed by evaluating end-of-life disposal strategies via a direct de-orbiting controlled re-entry from such Earth's target LEOs. Current directives require the risk of causality on the ground to be lower than 1 in 10,000. The main goal of the re-entry analysis is to perform simulations using the ESA DRAMA software to determine the on-ground risk caused by surviving fragments from spacecraft re-entering the Earth's atmosphere. These analyses are conducted with different inputs (solar activity, apogee, targeted perigee, assumed break-up altitude) to assess the variability of the impact footprint of all surviving fragments for different initial parameters. The target area for re-entry is the uninhabited South Pacific Ocean, and the spacecraft is modelled using the CROC (Cross Section of Complex Bodies) tool.

Keywords: debris mitigation, L2 Near Rectilinear Halo Orbit, genetic algorithm, Circular Restricted Three-Body Problem, controlled re-entry, footprint

Acronyms/Abbreviations

Lunar Orbital Platform-Gateway (LOP-G)
Near Rectilinear Halo Orbit (NRHO)
Earth-Moon L2 (EML2)
Federal Communications Commission (FCC)
Low-Earth Orbit (LEO)
Circular Restricted 3-Body Problem (CR3BP)
Differential Corrections (DC)
Periodic Orbit (PO)
State Transition Matrix (STM)
Lyapunov Orbit (LO)
Halo Orbit (HO)
Genetic Algorithm (GA)
South Pacific Ocean Uninhabited Area (SPOUA)
Argument of Perigee (AOP)
Spacecraft (SC)
Zero Velocity Surfaces (ZVS)
Jacobi Constant (JC)
Debris Risk Assessment and Mitigation Analysis (DRAMA)
Assessment of Risk Event Statistics (ARES)
Master Impact Flux and Damage Assessment (MIDAS)
Orbital Spacecraft Active Removal (OSCAR)
Cross Section of Complex Bodies (CROC)
Survival and Risk Analysis (SARA)
Two-Point Boundary Value Problem (TPBVP)
Ordinary Differential Equation (ODE)
Variable-Time Differential Correction (VTDC)
Reference System (RS)
European Organisation for the Exploitation of Meteorological Satellites (EUMETSAT)
EUMETSAT Polar System-Second Generation (EPS-SG)
Meteorological Operational Satellite - Second Generation (MetOp-SG)
End Of Life (EOL)

European Space Agency (ESA)
Spacecraft Atmospheric Re-Entry and Aerothermal Break-up (SCARAB)
Jet Propulsion Laboratory (JPL)

1. Introduction

In the era of space exploration and with the ambitious mission of establishing permanent human settlements on the Moon, the construction of the Lunar Orbital Platform-Gateway (LOP-G) in a Near Rectilinear Halo Orbit (NRHO) at the Earth-Moon L2 (EML2) Lagrange point has become an increasingly imminent reality [1],[9]. This initiative marks a significant increase in space traffic in the cislunar region, necessitating strict compliance with space debris regulations, such as the recent Federal Communications Commission (FCC) rule requiring deorbiting within 5 years to prevent contamination of this valuable space [2].

In response to these challenges, this paper introduces an alternative strategy for mitigating space debris generated by satellites positioned in NRHO orbits. Instead of adopting lunar surface impact as a disposal method, often unsustainable in the long term, this strategy proposes the transfer of spacecraft from NRHO orbits to Low-Earth Orbits (LEOs) and subsequent controlled re-entry into Earth's atmosphere.

This paper presents a comprehensive analysis divided into two distinct segments, each characterized by the employment of a different dynamic model. The initial part of the analysis was conducted using the Circular Restricted 3-Body Problem (CR3BP) through which it was possible to study the Halo orbit family that generates the starting 9:2 NRHO orbit and research the optimised re-entry trajectory with one or two impulses.

In the final part of the research, a dynamic atmospheric re-entry model is employed. In this way, the satellite is no longer considered as a material point, but as a body with a mass, size and composed of several subsystems in order to study its controlled re-entry and conduct a footprint sensitivity analysis.

The CR3BP offers a time-invariant system, specifically a collection of autonomous, epoch-independent equations that can be linearized to carry out Differential Corrections (DC) [3]. Therefore, in this dynamical model, it is possible to construct and validate Periodic Orbits (POs) using the simplest concepts of single-shooting methods and State Transition Matrix (STM).

This study delves into two distinct categories of periodic orbits: Lyapunov Orbits (LOs) which are characterized by their confinement to the same orbital plane as the two primary bodies, and Halo Orbits (HOs), which manifest as a three-dimensional extension originating from the Lyapunov orbits.

The aim of this analysis is to obtain the NRHOs for the Earth-Moon Lagrangian Point L2 (EML2) in the Earth-Moon binary system in order to define the starting orbit of the re-entry trajectory: the Southern L2 NRHO with 9:2 Lunar Synodic Resonance. The notation of 9:2 resonance indicates the relationship between the orbital period of the NRHO and the synodic period between Earth and the Moon. The selection of this particular resonance and NRHO for the Lunar Gateway is driven by considerations of stability, operational efficiency, and suitability for the intended space missions [4]. This orbit configuration minimizes the necessity for frequent corrective manoeuvres and significantly reduces extended periods of eclipse, rendering it a pragmatic choice for the Lunar Gateway, whether for a space station or an orbiting platform.

Given the starting orbit and its characteristics, the re-entry trajectory of the space debris from LOP-G orbit to 800 km LEO was performed. Re-entry trajectories from NRHO are particularly complex due to their dynamic instability and the numerous variables involved. These challenges necessitate the application of advanced algorithms, such as Genetic Algorithms (GAs), to successfully optimize re-entry trajectories while considering multiple objectives and constraints.

One of the distinctive features of GAs is their ability to perform optimization iteratively. This is particularly valuable when dealing with complex re-entry trajectories as it allows for progressively refining solutions to get closer to the desired goal.

Within the GA framework, solutions are represented as individuals, each characterized by a set of genes encoding crucial parameters defining the re-entry trajectory. Specifically, a set of 5 genes was utilized for the one-impulse re-entry trajectory, while the two-impulse trajectory employed 9 genes.

A carefully defined merit function has been employed to assess the quality of each individual in accordance with the specific objectives and constraints of the problem. This merit function has guided the selection process, identifying individuals with the greatest promise for reproduction. To avoid the selection of local optimal minima, the inclusion of crossover operators has allowed individuals to exchange genetic information through the combination of genes from selected parents. Furthermore, the mutation operator has been incorporated to introduce random variations in individual genes.

The application of genetic algorithms played a pivotal role in deriving the requisite initial conditions for integrating and propagating the re-entry trajectory. Through systematic analyses, a significant revelation emerged: a single impulse maneuver, even when supported by a lunar fly-by, proved to be insufficient for achieving Low-Earth Orbit (LEO) insertion. Instead, it was empirically demonstrated that a direct re-entry trajectory demanded a higher ΔV.

To surmount this challenge, a two-impulse strategy was formulated. The first impulse was introduced to harness

the inherent instability of the NRHO orbit, coupled with the lunar fly-by, resulting in a notable reduction of the initial ΔV (below 100 m/s) required to escape the lunar sphere of influence.

Nonetheless, achieving LEO insertion through the second impulse necessitated an additional ΔV expenditure of approximately 0.7 km/s, while ensuring final escape conditions at the Earth-Moon's Sphere of Influence (SOI). This intricate multi-step approach underscores the capacity of the genetic algorithm in elucidating an optimal trajectory, ultimately enhancing the feasibility of spacecraft re-entry from NRHO orbits into LEO.

Upon achieving the predetermined LEO altitude of 800 km, it was deemed appropriate to initiate a controlled re-entry strategy. This strategy entailed a sequence of Hohmann transfers to progressively lower orbits, culminating in the achievement of a sufficiently low perigee [5]. Subsequently, a final burn was executed to further reduce the perigee to sub-atmospheric levels, thereby compelling a controlled re-entry into Earth's atmosphere [6].

The concluding section of this paper focuses on the examination of the influence exerted by various orbital parameters have on the Controlled Re-entry phase over the South Pacific Ocean Uninhabited Area (SPOUA). This investigation leverages the ESA DRAMA tool and incorporates a dynamic model that considers the significant influence of the Earth's atmosphere and solar activity. Notably, this model extends beyond the approximation of a satellite as a material point, utilizing the EUMETSAT space agency's Metop-SG-A satellite as a reference for the study. The core objective of this research lies in the execution of simulations aimed at assessing the variability in the impact footprint concerning a range of initial parameters, encompassing solar activity, atmospheric drag, apogee, targeted perigee, Argument of Perigee (AOP), and the assumed breakup altitude.

2. Dynamical models

The CR3BP dynamical model employed in the first part of the analysis considers the spacecraft (SC) as a material point and is a simplification in which the only acting forces on the SC are those of the Earth and Moon. In the controlled re-entry analysis, due consideration is given to the spacecraft's mass, structure, components, as well as the inclusion of external aerodynamic forces such as Drag, Lift, Heat Flux, and Solar Activity. This approach enables a comprehensive analysis to be conducted.

2.1 The circular restricted three-body problem

A reasonable approximation to more accurate dynamical models of the Earth-Moon system, including those that might also include solar gravity, is provided by the dynamical model in the CR3BP. Within this specific application of the CR3BP, a thorough examination is conducted on the motion of a massless spacecraft under the gravitational forces exerted by the Earth and the Moon. These two primary celestial bodies are conceptually represented as point masses that follow circular orbits around their common barycenter. The spacecraft moves freely under the influence of the two primaries, and the spacecraft's motion is described relative to a coordinate frame, synodic reference system, which maintains synchronous rotation with the Earth-Moon system. By convention, quantities in the CR3BP are nondimensionalized such that the Earth–Moon distance, as well as the mean motion of the primaries, are both equal to a constant value of unity. In the context of the rotating frame, the scalar equations governing the spacecraft's motion can be mathematically expressed as [7]:

$$\ddot{x} - 2\dot{y} = \frac{\partial U}{\partial x},\ \ddot{y} - 2\dot{x} = \frac{\partial U}{\partial y},\ddot{z} = \frac{\partial U}{\partial z} \qquad (1)$$

where U is the pseudo-potential function.

No closed-form solution exists to the CR3BP equations of motion, but there are five equilibrium solutions, called libration points, that are usually denoted L_1 through L_5. Stable and unstable periodic orbit families, including the L_2 halo orbits, emerge in the vicinity of the libration points.

In the rotating frame, a conserved quantity termed the Jacobi constant $JC = 2U - v^2$ represents an energy-like integral of motion and it plays a pivotal role in constraining the motion of the spacecraft within regions of space where $v^2 > 0$ [1]. These regions are demarcated by zero velocity surfaces (ZVSs) that delineate the boundaries within which the spacecraft can manoeuvre freely. For Jacobi constant values exceeding that associated with the L_1 libration point, the ZVSs form closed regions around each of the two primaries. As the energy of the spacecraft trajectory increases, the Jacobi constant decreases progressively until, at the L_1 libration point, the ZVSs part at this location, granting the spacecraft the ability to transition between the two primaries. Similarly, when the value of the Jacobi constant decreases to the value associated with L2, the ZVSs open up at L2, allowing the spacecraft to depart entirely from the vicinity of the primary celestial bodies. In the case of spacecraft orbiting within one of the chosen Near Rectilinear Halo Orbits (NRHOs), the Circular Restricted Three-Body Problem (CR3BP) serves as a sound approximation for characterizing the trajectory's behaviour.

2.2 Controlled re-entry model

Within the realm of controlled re-entry analysis, a sophisticated model transcends the simplistic point-mass approximation, delving into the intricate dynamics between the spacecraft and Earth's atmosphere. This

advanced model duly acknowledges the paramount role played by atmospheric drag, a force of critical significance in shaping re-entry trajectories, but also the solar activity. The model meticulously incorporates the physical attributes of the spacecraft, encompassing mass, shape, and the intricate network of onboard subsystems in order to study how each component contributes to the re-entry trajectory in the SPOUA.

To rigorously evaluate the influence of diverse factors on the controlled re-entry phase, the ESA DRAMA (Debris Risk Assessment and Mitigation Analysis) tool was employed. This software tool enables ESA space programs to assess their compliance with the recommendations in the European Code of Conduct for Space Debris Mitigation. The DRAMA tool is a combination of several software tools all operating independently: ARES, MIDAS, OSCAR, CROC, SARA [8]. In the course of conducting this research, the utilization of CROC and SARA tools, was paramount. CROC served as the primary tool for spacecraft modelling and cross-section computation, while SARA played a crucial role in performing sensitivity analyses pertinent to controlled re-entry.

The methodology employed in this analysis embraced an "object-oriented" approach; at its core was the concept of a "parent spacecraft," a primary entity featuring a single well-defined primitive shape with the appropriate ballistic coefficient. Child components were integrated within parent components using the "contained-in" property, safeguarding them from atmospheric exposure. The "connected-to" property was employed to establish interconnections among parent components. This "object-oriented" methodology gave the spacecraft a structured representation, enabling thorough modelling, analysis, and sensitivity evaluations throughout the controlled re-entry procedure.

3. Periodic Orbits

The primary objective of this study is to develop a disposal trajectory originating from the LOP-G Near Rectilinear Halo Orbit (NRHO). To achieve this goal and establish 9:2 NRHO as the starting point for the disposal trajectory, this chapter outlines the methodologies employed for the construction and validation of Periodic Orbits within the framework of the Circular Restricted Three-Body Problem (CR3BP). Indeed, the NRHO orbits are perfectly periodic [3] within the confines of the three restricted circular bodies in the CR3BP framework.

Within the context of the CR3BP, a significant advantage is the system's time-invariant nature. It consists of a set of self-contained equations, free from dependence on specific epochs, facilitating linearization for differential corrections. This study focuses on two distinct categories of periodic orbits: Lyapunov Orbits, characterized by their co-planar alignment with the two primary bodies, and Halo Orbits, a three-dimensional offshoot originating from the Lyapunov family.

In addressing the initial stability requirements and refining the preliminary estimations that can be derived through analytical approaches, this study employs more straightforward techniques. Specifically, it utilizes methods like single-shooting Differential Corrector (DC) strategies. These methods offer a simpler, yet highly effective, approach to enhancing the accuracy of initial trajectory approximations.

3.1 Differential correctors

Determining a trajectory from $\tilde{X}(\tau_0)$ to a desired point $\tilde{X}(\tilde{X}(\tau_0), \tau_f)$ can be approached in the simplest manner by selecting an acceptable initial state and evolving it over time while introducing random or discrete adjustments to the initial state until the desired point is reached. However, this blind trial-and-error approach lacks the ability to assess whether changes in the initial values contribute to improved convergence [3]. To address this limitation and enhance the reliability of trajectory determination, it is crucial to comprehend how to modify and correct the initial state $\tilde{X}(\tau_0)$ to achieve the desired final state. An effective framework for achieving this understanding is the Two-Point Boundary Value Problem (TPBVP). This approach focuses on comprehending the impact of initial conditions on final conditions, thereby providing a more robust methodology for trajectory calculation.

Hence, the objective is to quantify the disparity between the desired and actual final states, described as follows:

$$\delta\tilde{\boldsymbol{X}}(\tau_f) = \tilde{\boldsymbol{X}}(\tilde{\boldsymbol{X}}(\tau_0), \tau_f) - \widetilde{\boldsymbol{X}^*}(\widetilde{\boldsymbol{X}^*}(\tau_0), \tau_f) \qquad (2)$$

To eliminate these differences between the two states, the differential correction procedure is employed. It is noteworthy that a specific correction to the initial state, denoted as $\delta\tilde{X}(\tau_0)$, should yield the desired initial state as:

$$\widetilde{\boldsymbol{X}^*}(\tau_0) = \tilde{\boldsymbol{X}}(\tau_0) + \delta\tilde{\boldsymbol{X}}(\tau_0) \qquad (3)$$

Therefore, the introduction of the State Transition Matrix (STM), also known as the sensitivity matrix, plays a crucial role in this context:

$$\delta\tilde{\boldsymbol{X}}(\tau_f) = \tilde{\boldsymbol{\Phi}}(\tau_f, \tau_0)\ \delta\tilde{\boldsymbol{X}}(\tau_0) \qquad (4)$$

The STM ($\tilde{\Phi} \in \mathbb{R}^{6x6}$) serves as a linear mapping within the CR3BP domain and provides insights into how sensitive the final state is to variations in the initial state. Essentially, it measures the degree of convergence or divergence of these variations concerning a reference solution.

The STM evolves over the trajectory in a manner similar to the trajectory itself, and it is governed by its own set

of 36 ordinary differential equations (ODEs) that describe this evolution:

$$\dot{\tilde{\Phi}}(\tau, \tau_0) = \tilde{A}(\tau)\, \tilde{\Phi}(\tau, \tau_0) \qquad (5)$$

where $\tilde{A}(\tau)$ represents the Jacobian matrix and is a function of the state of the reference trajectory.
In the context of trajectory optimization, a variable-time shooting method known as Variable-Time Differential Correction (VTDC) is employed. This method considers the integration time, which could represent the period required for a full revolution around a specific PO. The design vector $\tilde{X}(\tau_0)$ encompasses state variables, including the integration time, and plays a crucial role in evaluating the impact of time variation on the final state:

$$\tilde{X_0} = \{\xi \quad \eta \quad \zeta \quad \dot{\xi} \quad \dot{\eta} \quad \dot{\zeta}\} \qquad (6)$$

Using these specific values results in the Jacobian, which represents the derivative of state variables concerning other state variables. Consequently, there are seven free-variables and six constraints. This combination introduces an additional column in the Jacobian matrix, making it $\tilde{J} \in \mathbb{R}^{6x7}$ in its entirety.

3.3 Computation of Planar Lyapunov Orbits in the CR3BP

Lyapunov orbits are characterized by their planar nature within the $\hat{\xi}$-$\hat{\eta}$ plane in the CR3BP's synodic Reference System (RS), meaning they don't have components in the out-of-plane direction.
The straightforward computation of Lyapunov orbits involves the construction of an appropriate design vector and constraint vector tailored to these orbit characteristics. When a Lyapunov orbit intersects the $\hat{\xi}$-$\hat{\zeta}$ plane, it necessitates that this intersection remains perpendicular after half of its orbital period, yielding a simple constraint vector $\{\eta \;\; \dot{\xi}_f\} = 0$.
The free-variable vector, encompassing initial position along the $\hat{\xi}$ axis, initial velocity along the -$\hat{\eta}$ direction and integration time τ, allows for targeted adjustments during computation:

$$\tilde{X}_0 = \begin{Bmatrix} \xi \\ \dot{\eta} \\ \tau \end{Bmatrix} \qquad (7)$$

The Jacobian matrix, crucial in the differential correction process, can be directly calculated by finding the associated partial derivatives.
In the following Fig. 1, a complete family of Lyapunov orbits orbits (LOs) for the EML2 is presented is presented, with $A_y = 1 \times 10^4$ km [3] (elliptical black shapes centered in L2). The procedure to obtain these orbits involved incrementally adjusting the ξ_0 value by a finite step $d\xi$, which remained constant throughout the differential correction (DC) process. This allowed for variations in the initial η and integration time τ, while maintaining ξ_0 constant during DC.

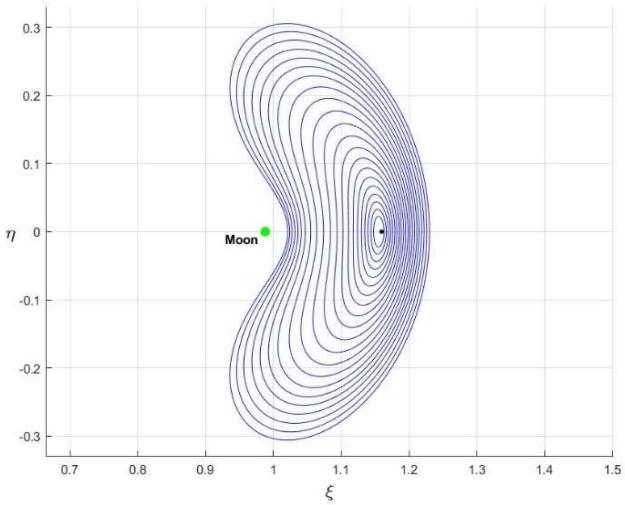

Fig. 1. Family of LOs for the EML2

These orbits initiate from L2 and showcase (Fig. 2) varying Jacobi constants (JC), reflecting differences in complexity. Smaller orbits closely resemble elliptical shapes, while larger orbits exhibit the distinctive cashew shape, illustrating the greater mechanical energy requirements associated with traversing more intricate geometries.

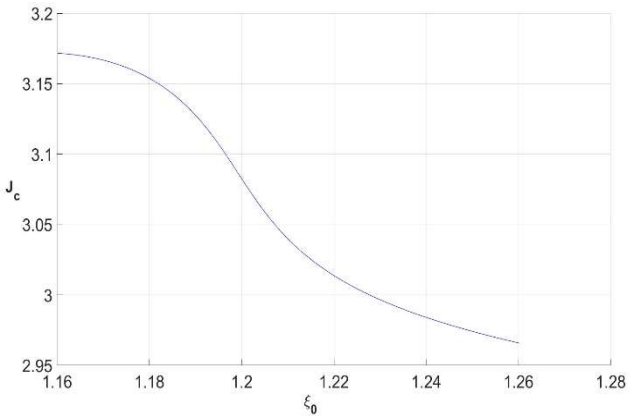

Fig. 2. EML2 LOs Jacobi Constant

3.4 Computation of Halo Orbits in the CR3BP

Halo orbits (HOs) are three-dimensional and originate from the bifurcation of LOs at specific Jacobi Constant levels associated with the EML2 binary system. Of particular significance are the Near Rectilinear Halo

Orbits (NRHOs) due to their prospective utilization in upcoming space missions. Specifically, the aim is to identify the LOP-G NRHO orbit with a 9:2 Lunar Synodic Resonance. Synodic resonance (SR) is a key concept in understanding NRHOs. An x:y synodic resonance indicates that a spacecraft (SC) on such a 3D periodic orbit completes x revolutions while the nearest primary body completes y full periods. In the EM system, the Moon's period with respect to a fixed star is the sidereal month of 27.32166 days [3].

The inclusion of the third dimension in the constraint and free-vector is essential for characterizing HOs. This occurs due to the planar bifurcation, which is influenced by the initial position with a negative out-of-plane component ξ_0, while the out-of-plane velocity is constrained to be zero. Consequently, the constraint vector for a HO is $\{\eta \;\; \dot{\xi}_f \;\; \dot{\zeta}_f\} = 0$.

The free-variable vector, which encompasses the initial position along the $\hat{\xi}$ axis and $\hat{\zeta}$ axis, the initial velocity along the $-\hat{\eta}$ direction, and the integration time τ, provides the flexibility for targeted adjustments during computation:

$$\widetilde{\boldsymbol{X}}_0 = \begin{Bmatrix} \xi \\ \zeta \\ \dot{\eta} \\ \tau \end{Bmatrix} \tag{8}$$

Starting with an LO of $A_y \approx 3 \times 10^4$ km [3], the complete set of Halo orbits, leading up to the 9:2 NRHO orbit utilized in this re-entry analysis, is illustrated in the Fig.3.

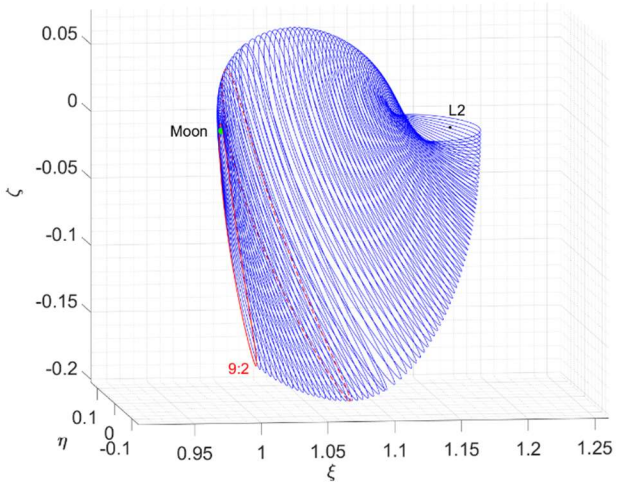

Fig. 3. Family of HOs for the EML2

For the exportation of this Halo family, a continuation strategy with distinct steps was employed. Initially, starting from the LO, small $\delta\zeta$ steps were applied to decrease the out-of-plane position ζ_0, enabling the search for other values of the free-vector. When the HOs approached a nearly vertical orientation, adjustments were made to decrease the axial position ξ_0 of the small $\delta\xi$ steps. To locate the final NRHOs, further alterations were introduced in the ζ_0 position. This multi-step approach allowed for a comprehensive exploration of the Halo orbits.

When examining Jacobi's constant (JC) in Fig.4, it becomes evident that it does not follow a uniform trend. In the proximity of EML2, the JC exhibits its highest values, signifying lower energy levels. As the HO approaches a near-vertical configuration, the JC experiences a decline, reaching its minimum at the dashed NRHO. Beyond this juncture, JC begins to rise once more, ultimately reaching the value associated with the 9:2 NRHO.

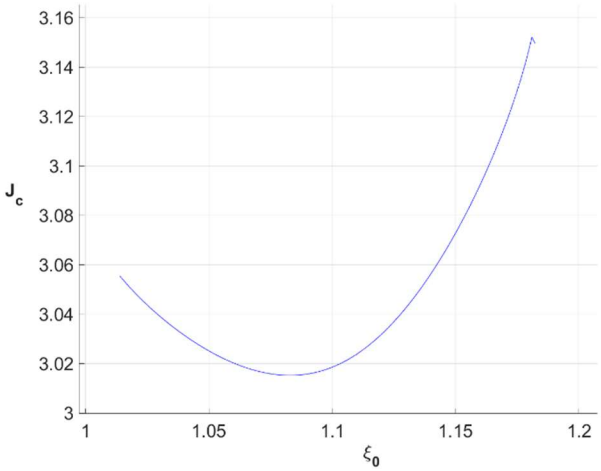

Fig. 4. EML2 HOs Jacobi Constant

Hence, it is evident that through this comprehensive exploration, every state corresponding to the 9:2 NRHO is obtained. The initial state of this 9:2 NRHO is delineated as follows:

$$\widetilde{\boldsymbol{X}}_0 = \{1.0139, 0, -0.1758, 0, -0.0848, 0\}$$
$$\boldsymbol{\tau} = 1.4024 \qquad \boldsymbol{JC} = 3.0555$$

4. Genetic algorithm

One of the distinctive features of Genetic Algorithms (GAs) is their ability to perform optimization iteratively. This is particularly valuable when dealing with complex trajectories as it allows for progressively refining solutions to get closer to the desired goal.

Re-entry trajectories from NRHO are particularly complex due to their dynamic instability and the numerous variables involved. Other optimization techniques were found to be overly sensitive to initial conditions and unable to meet the imposed constraints, thus leading to the adoption of a genetic algorithm.

Genetic algorithms use a vocabulary rich in terms of biological nature [10],[11]. They speak of individuals (or

genotypes, structures) of a population. Individuals, in turn, are made up of a certain number of units, called genes (or also characters, decoders) arranged in a linear succession. Each gene is capable of influence the behaviour of one or more individuals. The genes of a certain individual are arranged in certain positions called string positions. Therefore, each individual represents a potential solution to the problem.
The algorithm starts the search from an initial random population of individuals. This search has a dual purpose: to calculate the best solution and to explore the space of potential solutions. During a generation, the algorithm maintains a population of potential solutions and each individual is assigned a merit value, a value that measures its goodness and, subsequently, by calculating the best individuals and through genetic operators such as crossover, mutation, etc, a new population is created.
A GA is built from a variety of unique elements. This is a particular strength because it allows for the reuse of standard components in numerous GAs with minimal adaptation, simplifying implementation. The key elements are the individuals encoding, the merit function, selection, recombination and the evolution scheme.

4.1 Individuals encoding

The encoding scheme plays a significant role in the majority of computational problems. The provided data must be encoded in a specific bit string. Depending on the problem domain, different encoding schemes [12] are used. Binary, octal, hexadecimal, permutation, value-based, and tree are some common encoding schemes.
In this research, the adoption of value encoding was chosen, specifically representing orbital parameters crucial for the subsequent trajectory implementation, as elucidated below. The forthcoming chapter delves into the examination and exploration of two distinct re-entry trajectory types: short-duration and long-duration solutions; these comprise direct re-entry trajectories necessitating a singular high ΔV impulse and split trajectories involving two low ΔV impulses, respectively. Additionally, this genetic approach applies the boundary problem principle, wherein each gene within an individual's genetic makeup is selected within predefined lower and upper parameter limits, distributed randomly between these boundaries. In the case of a single impulse trajectory, an individual comprises 5 genes arranged as follows:

ΔV	T_{halo}	α	β	$T_{trajectory}$

- ΔV represents the amount of velocity that must be added to the spacecraft's initial velocity at the starting point of the Halo orbit to transition from the starting orbit to reach a Low Earth Orbit (LEO);
- T_{halo} which is the time t_1 at which the first pulse on the NRHO is provided. Considering the aposelenium of the NRHO as time t_0, this gene makes it possible to define how long the NRHO has covered before the first manoeuvre is performed. It leverages the instability of the Halo orbit to break free from the lunar sphere of influence;
- α Denotes the angle formed between the spacecraft's velocity vector and the direction of thrust applied by the spacecraft's propulsion within the plane of the velocity vector, I.e. the in-plane thrust direction;
- β, represents the angle formed between the spacecraft's velocity vector and the direction of thrust applied by the spacecraft's propulsion in a direction perpendicular to the plane of the velocity vector, I.e. the out-of-plane thrust direction;
- $T_{trajectory}$ signifies the propagation time of the trajectory, essentially defining the duration of the entire mission once the two variables, defining the two distinct trajectory arcs, are summed up.

Hence, following the determination of the starting point of the Halo orbit via the second gene, T_{halo} , the initial velocity vector, encompassing all its components within the synodic system, becomes ascertainable. Subsequently, it becomes feasible to compute the angle between the velocity vector and the local horizon within the velocity vector plane:

$$a = \tan^{-1}(\dot{\eta}, \dot{\xi}) \qquad (9)$$

and the angle between the velocity vector and the local horizon in a direction perpendicular to the plane of the velocity vector:

$$b = \sin^{-1}(\dot{\zeta}, v_{syn}) \qquad (10)$$

Here, v_{syn} represents the magnitude of velocity in the synodic system that the spacecraft possesses on the Halo orbit at the starting point. To establish the direction of thrust and subsequently compute the various components of the ΔV vector, the third and fourth genes, α and β angles, are incorporated by adding them to the previously mentioned angles, a and b.
Instead, in the case of a re-entry trajectory with two impulses, an individual consisting of 9 genes was utilized, structured as follows:

ΔV_1	T_{halo}	α_1	β_1	$T_{trajectory1}$	ΔV_2	α_2	β_2	$T_{trajectory2}$

In this context, the interpretation of each parameter remains consistent with the descriptions provided earlier, with the distinction that subscript 1 pertains to the trajectory arising from the first impulse, while subscript 2 pertains to that originating from the second.

4.2 Merit function

The merit function assumes a pivotal role within the algorithm, serving as the driving force that guides the selection of the most meritorious individual in each iterative step. Its importance lies in its capacity to evaluate and quantify how well each potential solution aligns with the desired objectives and constraints of the optimization problem**.** A well-crafted merit function encapsulates the essence of the optimization problem, encapsulating the criteria for success or efficiency. It provides a means to assess and rank individuals within the population based on their ability to meet the defined goals. In essence, the merit function acts as the compass, directing the genetic algorithm toward improved solutions with each generation.

The merit function, at its core, is a multi-objective entity that encapsulates a range of criteria, objectives, and constraints within the optimization problem. This multi-objective framework is instrumental in addressing complex real-world scenarios where there may be conflicting goals and trade-offs to consider. An integral aspect of the multi-objective merit function is the assignment of different weights to each objective or constraint. These weights serve to reflect the relative importance of each criterion within the optimization problem.

In this research, the merit function is constructed as a multi-objective framework comprising three distinct objectives, each of which is described below, with weights assigned in order of significance:

1. *Altitude Objective* (*Highest Weight*): the primary objective is to attain an altitude of 800 kilometers above Earth's surface. This objective is accorded the highest weight within the merit function. Reaching the desired altitude is of utmost significance, as it serves as the established criterion for initiating controlled re-entry maneuvers and securing the arrival at the designated SPOUA target area;

2. *Velocity Objective* (*Intermediate Weight*): the second objective is to attain a circular velocity equal to that of Low Earth Orbit (LEO) at 800 kilometers;

3. *Delta-V Minimization Objective* (*Lowest Weight*): the third objective is to minimize the required ΔV for the trajectory. This objective is assigned the lowest weight among the three. Minimizing ΔV is desirable as it contributes to fuel efficiency and cost-effectiveness, but it is considered secondary as it is already limited by the definition as input of the maximum and minimum value of the respective gene.

In this optimization process, these objectives are further transformed into error terms, which are used to quantify the discrepancy between the target goal and the outcome achieved by each individual within the gene pool. These error terms essentially represent how well or poorly an individual solution aligns with the predefined mission objectives. The conversion of these objectives into error terms facilitates the establishment of a quantitative performance metric for every candidate trajectory, thereby initiating the commencement of the selection process.

4.3 Selection

The selection component of a GA is designed to use merit to guide the evolution of individuals by selective pressure. Therefore, the selection operator specifies which parents choose to create the next generation. Individuals are therefore selected for recombination based on merit. Those with higher merit should have a greater chance of selection than those with lower merit, thus creating a selective pressure towards more highly fit solutions. Selection is usually with replacement, meaning that highly fit individuals have a chance of being selected more than once or even recombined with themselves.

In the execution of the genetic algorithm applied in this study, the selection method chosen was the Roulette Wheel selection. This process entailed reordering the individuals based on their merit values, incorporating the elitist approach. Under this strategy, only the top-performing 30% of individuals advanced to the subsequent generation. Following this selection, genetic operators such as crossover and mutation were applied to this selected subset, effectively generating the complete new generation of candidate trajectories.

4.4 Recombination

Recombination is the fundamental process through which individuals, drawn from a source population, are combined to generate members of a succeeding population. This process emulates the genetic material mixing that transpires during reproduction in organisms. Notably, the selection for recombination is inclined towards favouring individuals with higher merit values, with the anticipation that this bias will ultimately lead to the evolution of more highly fit individuals. Recombination comprises two primary components: genetic operators known as crossover and mutation. It is essential to acknowledge that genetic operators exhibit non-deterministic behaviour in their operation.

The *crossover* operator embodies the mixing of genetic material derived from two selected parent individuals, resulting in the creation of one or two offspring individuals. The application of the crossover operator encompasses several methods, with one widely employed approach being the one-point crossover. In this method, an integer n, randomly selected from the range of 1 to the total number of genes constituting the individual, is utilized. The offspring is generated by merging the elements of individual 1 located in positions lower than n with the elements of individual 2 situated in positions higher than n.
Within the implemented Genetic Algorithm (GA) of this study, a one-point crossover strategy was employed, incorporating three dice rolls to facilitate this process:

- *DICE 1*: this die randomly determines the index, denoted as '*n*', at which the genetic material exchange or "cut" will take place within the individual. The range of possible values for 'n' spans from 1 to the length of the individual;

- *DICE 2*: The second die is responsible for the random selection of Parent 1. Specifically, it chooses Parent 1 from among the elite individuals that have successfully advanced to the subsequent generation;

- *DICE 3*: Similarly, the third die is responsible for the random selection of Parent 2. It also selects Parent 2 from the pool of elite individuals who have progressed to the next generation.

Additionally, a constraint was imposed within the algorithm, specifically that if the outcomes of dice 2 and dice 3 were identical, the selection process would be repeated until distinct outcomes were obtained. These dice rolls are integral to the one-point crossover process and introduce an element of randomness, ensuring diversity and adaptability within the genetic algorithm. By employing such a mechanism, the GA can explore a broader solution space and enhance the potential for discovering optimal trajectories.
In contrast, the *mutation* operator plays a pivotal role in preserving genetic diversity as the population transitions from one generation to the next. Mutation serves as a mechanism to sustain genetic variability within the population, preventing the algorithm from prematurely converging to a suboptimal solution by ensuring exploration of a broader solution space.
In the context of this study, every chromosome position within the individual undergoes the standard mutation operator. The process entails generating a uniform probability random number within the range [0,1] and subsequently comparing its value with a predefined "mutation rate." Conventionally, mutation rates are set at very small values, such as 0.1. If the randomly generated number surpasses the mutation rate, no mutation is applied at that particular position. However, if the mutation rate equals or exceeds the random number, the mutation techniques are activated, introducing variability and adaptability into the genetic material. This stochastic process is vital in enhancing the algorithm's capacity to explore and exploit a wider spectrum of potential solutions.
In the scope of this research, an additional die was introduced to facilitate random genetic mutation. The mutation process employed an arithmetic averaging approach, wherein the genes' value of parent 1 and parent 2 were averaged to introduce variability into the offspring. DICE 4 was implemented as follows:

- DICE 4: This die randomly generates a number representing the probability of mutation. Subsequently, it is compared with the predefined 'mutation rate,' which was set at 0.05 in this case. Consequently, a mutation is executed on an individual only if the fourth die produces a number lower than the mutation rate;

However, it is crucial to exercise caution in managing the mutation rate, as its value significantly influences the algorithm's behaviour. An excessively high mutation rate can lead to rapid loss of valuable genetic information within the population, hindering the convergence to optimal solutions. Conversely, an excessively low mutation rate may diminish the GA's effectiveness in generating new solutions and diversifying the population. Furthermore, in a deliberate effort to enhance genetic diversification, it was decided to introduce approximately 5% of new individuals with each generation. These new additions were positioned as the final individuals within the new generation, and the value of each gene was selected in accordance with the method outlined in chapter 4.1.

5. Controlled Re-entry Analysis

In pursuit of conducting a comprehensive controlled atmospheric re-entry analysis, the EPS-SG A satellite, operated by the space company EUMETSAT, was chosen as the focal subject. To perform this study, the satellite was modelled utilizing the CROC tool, as depicted in Fig. 5. This virtual representation of the satellite encompassed a total mass of *2722.03* kg, with a complex structure composed of *418* individual components. To streamline the modelling and analysis process, these components were thoughtfully categorized into distinct subsystems, establishing hierarchical relationships between parent and child components.

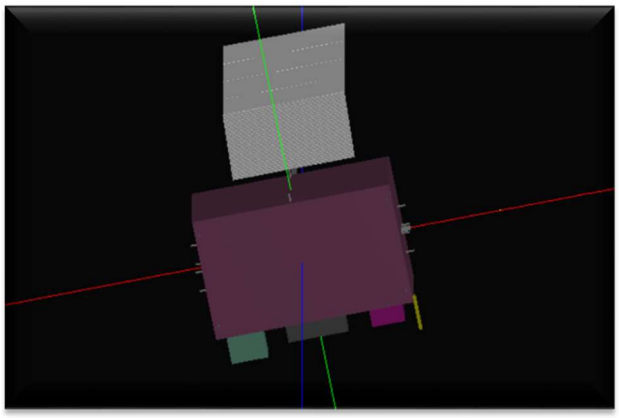

Fig. 5. EPS-SG A model by CROC

After reaching an altitude of 800 km, the controlled re-entry maneuver is executed with the primary objective of precise targeting within the predefined SPOUA region. This designated area, delineated by longitudinal coordinates spanning from -175 to -85 degrees and latitudinal boundaries extending from -60 to -30 degrees, serves as the focal point for re-entry operations.
The strategy involves executing a series of Hohmann transfers to lower orbit until a sufficiently low perigee from which the very last burn would bring the perigee further down to a sub-atmospheric altitude, forcing re-entry [5]. Notably, the precise positioning of the perigee, particularly in terms of its argument of latitude, emerges as a critical factor in defining the conclusive burn. To ensure the satellite's optimal re-entry trajectory aligns with a descending pass, the argument of latitude is meticulously set at 240 degrees for the nominal case [6]. The characteristics of the orbit in the nominal after the last burn are presented in Table 1.

Table 1. Orbit after the last burn

MEAN ORBITAL ELEMENTS	AFTER LAST BURN
Begin date	2030/07/31 12:00:00
Perigee altitude	30
Apogee altitude	780
Semi-major axis	6783.138
Eccentricity	0.05528415
Inclination	98.701
RAAN	220
AOP	240
Mean anomaly	180

6. Results and Discussion

6.1 Re-entry trajectory from NRHO to LEO

In the case of the one-impulse trajectory, it's essential to highlight that it was not optimized, primarily due to the limitations posed by the lunar flyby. The lunar flyby, while effective in reducing the initial ΔV requirement, does not allow the target orbit to be reached directly. Consequently, the direct transition to the Low-Earth Orbit (LEO) target orbit with a single impulse becomes unfeasible within the constraints of the lunar flyby. To achieve this transition directly, a considerably larger ΔV is necessary. Once the LEO target orbit is reached, a subsequent circularization maneuver with a ΔV of 2.7087 km/s is executed to circularize the trajectory. The direct re-entry trajectory, generated within the synodic reference system, is illustrated in Fig. 6. Furthermore, the outputs obtained from the genetic algorithm are highlighted in the Tab.2 below for reference.

Tab. 2: Output GA for single impulse trajectory in the Synodic RS

	ΔV	T_{halo}	α	β	$T_{trajectory}$
ONE-IMPULSE t_1	*[km/s]*	*[rad]*	*[deg]*	*[deg]*	*[rad]*
	0.864	*1.382*	*162.7*	*169.0*	*1.005*

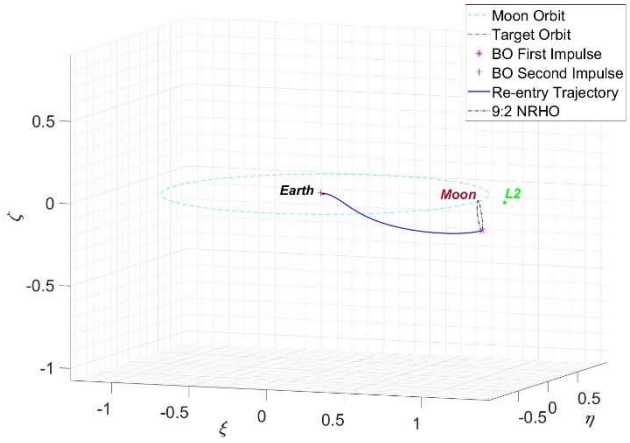

Fig. 6. One-pulse Re-entry trajectory in the Synodic RS

In light of this revelation, the implementation of a second impulse became necessary. The two-pulse trajectory approach emerges as a robust and viable strategy for effecting the transition from NRHO to LEO. By leveraging the genetic algorithm optimization process, this method optimally balances mission objectives, fuel efficiency, and trajectory feasibility, ultimately enhancing the feasibility of spacecraft re-entry from NRHO orbits into LEO.
Furthermore, it should be emphasised that, upon reaching the target orbit_by an altitude of 800 kilometers and a velocity closely approximating the corresponding circular velocity, an additional circularization pulse was executed.
A temporal reference was established, with t_0 marking the spacecraft's position at the aposelenium of the Halo orbit. Subsequently, time t_1 signified the start of the first propulsion pulse on the Halo orbit, while time t_2 marked

the initiation of the second propulsion pulse. Finally, time t_3 represented the execution of the last pulse necessary for achieving circularization. The trajectory generated in the synodic reference system visually illustrates this temporal progression, as depicted in Figure 7. The optimized results yielded by the genetic algorithm are summarized in Tables 3 and 4:

	ΔV_1	T_{halo}	α_1	β_1	$T_{trajectory1}$
FIRST IMPULSE t_1	*[km/s]*	*[rad]*	*[deg]*	*[deg]*	*[rad]*
	0.0903	*0.2643*	*306.6*	*-94.42*	*7.6258*

Tab. 3: Output GA for first impulse in the Synodic RS

	ΔV_2	α_2	β_2	$T_{trajectory2}$
SECOND IMPULSE t_2	*[km/s]*	*[deg]*	*[deg]*	*[rad]*
	0.7237	*305.84*	*-178.19*	*0.44325*

Tab. 4: Output GA for second impulse in the Synodic RS

To these two ΔV values, an additional ΔV of 2.23 km/s for circularizing the LEO orbit must be considered.

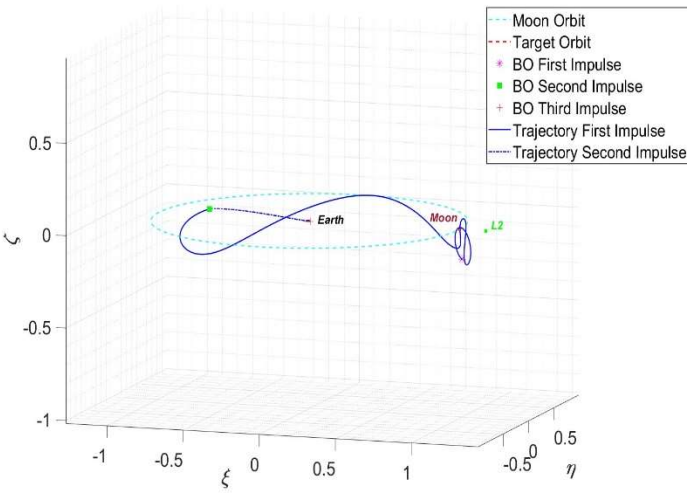

Fig. 7. Two-pulse Re-entry trajectory in the Synodic RS

In the analysis of the initial impulse, a specific focus was placed on the evasion of the lunar sphere of influence, as illustrated in Fig. 7. By adeptly harnessing the lunar influence, a lunar fly-by was executed, leading to a significant reduction in the ΔV expenditure required for the trajectory. This optimization was achieved by implementing a precise perturbation to the NRHO orbit, generating acceleration during the first quarter of the orbit from aposelenium. The re-entry trajectory is best observed in Fig. 7 in the inertial reference system, and it can also be comprehended by examining the velocity profile throughout the re-entry trajectory, as depicted in Fig. 8.

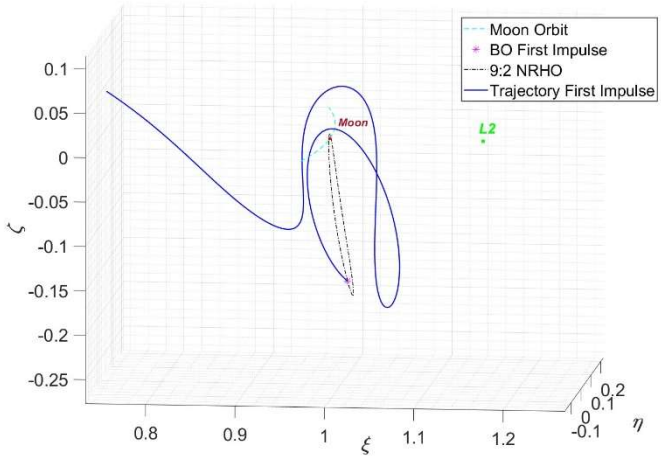

Fig. 6. Lunar leading-side fly-by in the Synodic RS

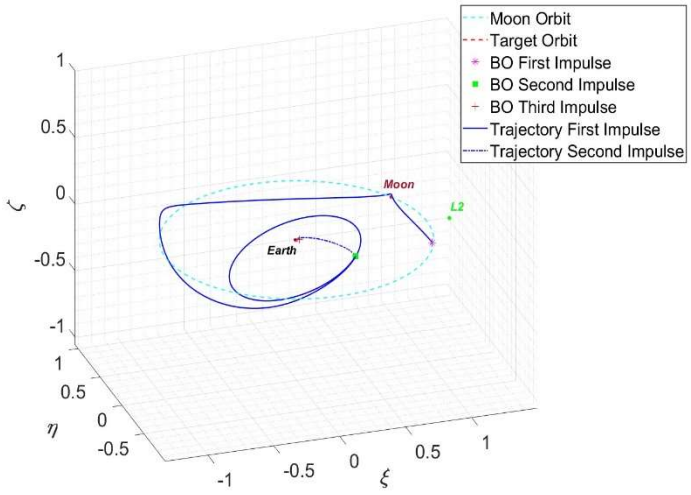

Fig. 7. Two-pulse Re-entry trajectory in the Inertial RS

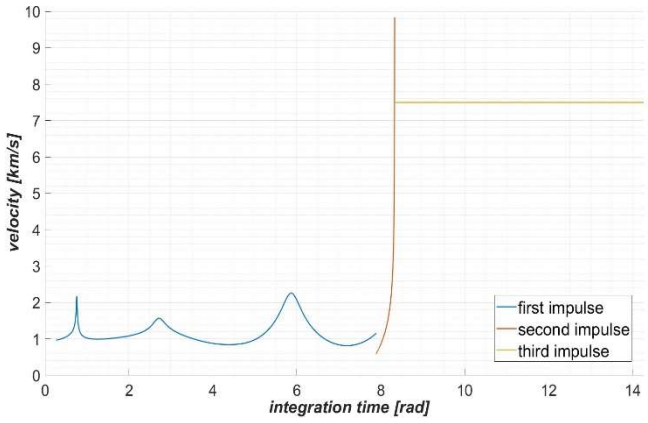

Fig. 8. Velocity in the Inertial RS

6.2 Sensitivity Analysis for the Controlled Re-entry

Different scenarios of different dispersion levels are simulated to illustrate the sensitivity of the footprint concerning the considered uncertainties in the initial parameters. This analysis aims to demonstrate how different degrees of uncertainty influence the resulting footprint, highlighting the importance of accurately characterizing the initial conditions in controlled re-entry simulations.

6.2.1 Argument of perigee

The AOP stands out as a crucial parameter with significant sway over the footprint's position, as demonstrated by Tab. 5, and it emphasizes the importance of meticulous parameter management and adjustment throughout End-Of-Life (EOL) planning and execution. To achieve precise targeting of the SPOUA, it becomes evident that maintaining the AOP within the approximate range of 235 to 255 degrees is fundamental. For a comprehensive understanding of the Argument of Perigee's impact on the footprint, a thorough exploration was conducted by varying this parameter across a range from 0 to 360 degrees.

Tab. 5. Results of the sensitivity analysis for AOP

AOP					
	235°	*240°*	*245°*	*250°*	*255°*
Min Latitude	*-37.47*	*-42.80*	*-48.82*	*-54.78*	*-60.55*
Max Latitude	*-29.34*	*-34.85*	*-41.44*	*-46.19*	*-51.68*
Min Longitude	*-106.26*	*-107.84*	*-109.78*	*-112.25*	*-115.54*
Max Longitude	*-104.07*	*-105.25*	*-106.67*	*-108.38*	*-110.48*

It's essential to note that within this analysis, the designated break-up altitude was established at 78 km above Earth's surface, with a corresponding perigee altitude of 30 km (assuming Equator Radius). As depicted in Fig. 9, the Earth's oblateness introduces a noteworthy effect on the footprint's dimensions. Specifically, the footprint exhibits a narrower profile at the equatorial regions and expands as it reaches higher latitudes.

This phenomenon can be attributed to the Earth's oblateness causing a reduction in the angle at which the spacecraft intersects the break-up altitude as latitude increases. Consequently, the normal component of velocity at this intersection is lower than it would be at the equator.

Consequently, this leads to a lengthier footprint due to both the greater expanse of Earth's atmosphere traversed by the space debris and the reduced normal velocity, culminating in an extended trajectory duration and dispersion of debris.

Furthermore, Fig.9 illustrates that the latitude of the footprint consistently precedes the respective latitude value corresponding to the Argument of Perigee, owing to the proximity of the perigee altitude (30 km) to the break-up altitude (78 km). This observation underscores the intricate interplay between various parameters and their cumulative effect on the re-entry footprint's characteristics.

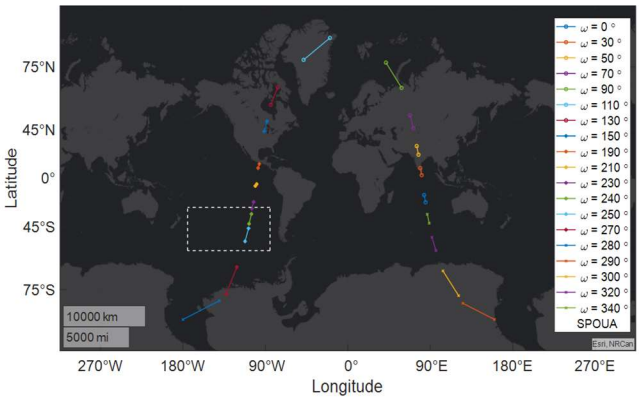

Fig. 9. Global sensitivity analysis for different AOP

6.2.2 Perigee Altitude

The perigee altitude emerges as another pivotal parameter significantly influencing the position and dimensions of the footprint due to its close correlation with the break-up altitude. Subsequent combined analyses will explore diverse perigee altitude values, holding the break-up altitude at a consistent 78 km while keeping other parameters at their nominal settings. This analysis underscores how the re-entry angle - defined as the angle between the post-final burn orbit and the break-up altitude - exerts a pronounced influence on the footprint. Specifically, lower perigee altitudes yield considerably shorter footprints due to their higher re-entry angles and normal velocity components, as compared to perigee altitudes approaching the break-up altitude. Furthermore, there's a non-linear increase in downrange distance, particularly as the perigee altitude converges toward 78 km, as illustrated in Fig. 10.

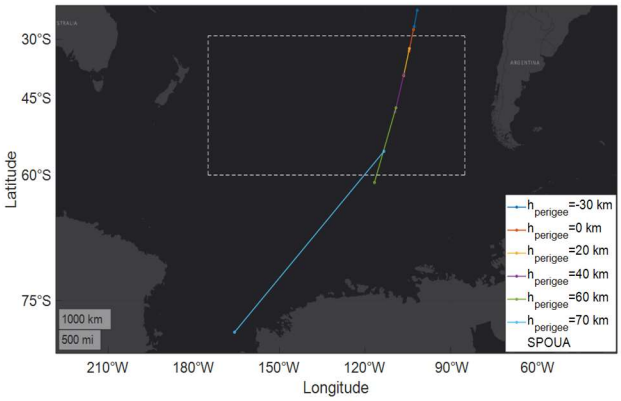

Fig. 10. Sensitivity analysis for different Perigee Altitude

6.2.3 Apogee Altitude

Another sensitivity analysis involves the evaluation of apogee altitude while maintaining the perigee and all other parameters at their nominal values. The results reveal minimal variations when altering the apogee altitude within the range of 250 km to 2000 km. These alterations predominantly manifest as a southward shift in the footprint's position with increasing altitude, accompanied by an enlargement in size. However, these shifts remain confined in scale. Consequently, it becomes apparent that maintaining a consistent apogee altitude from the starting circular orbit is a viable strategy, allowing for potential fuel conservation without necessitating apogee altitude adjustments.

6.2.4 Solar Activity

Another crucial aspect is the impact of solar activity on the footprint's characteristics. Simulation results have demonstrated significant deviations depending on the position within the solar cycle at which the simulation commences. Additionally, the level of solar activity, whether high, medium, or low, can exert a considerable influence on the outcomes.

Within the air density models available in ESA DRAMA, solar activity is parameterized using the solar radio flux F10.7, denoting the solar radio emission flux density at a wavelength of 10.7 cm. The analysis encompassed Solar Flux values ranging from $100 \cdot 10^{-22}$W/m^2/Hz to $500 \cdot 10^{-22}$ W/m^2/Hz. It's essential to emphasize that, in all these analyses, the break-up altitude was consistently set at 78 km.

However, analysing the scenarios with perigee altitudes of 30 km and 50 km, it becomes evident that the footprints display minimal variations across different Solar Flux values. Indeed, at these specific altitudes the influence of solar activity on atmospheric density remains notably minor. This phenomenon is attributable to the complex interplay of factors affecting the satellite's drag acceleration during atmospheric re-entry, which hinges on variables including atmospheric density (ρ), spacecraft cross-sectional area (A), spacecraft mass (m), relative velocity to the atmosphere (v), and the drag coefficient (C_D):

$$a_D = -\frac{1}{2}\rho\frac{A\,c_D}{m}v^2 \qquad (11)$$

In the analysis conducted at varying perigee altitudes, the primary factors affected at the break-up altitude are the re-entry angle and velocity. In cases with perigee altitudes of 30 km and 50 km, higher velocity prevails over density variations due to solar activity, resulting in nearly overlapping footprints with minimal sensitivity to solar activity. However, in the case of a 70 km perigee altitude (Fig. 11), solar activity and atmospheric density have a more pronounced impact on the footprint, leading to cross-track dispersion despite reduced re-entry velocity. This demonstrates significant sensitivity to solar activity in this particular scenario.

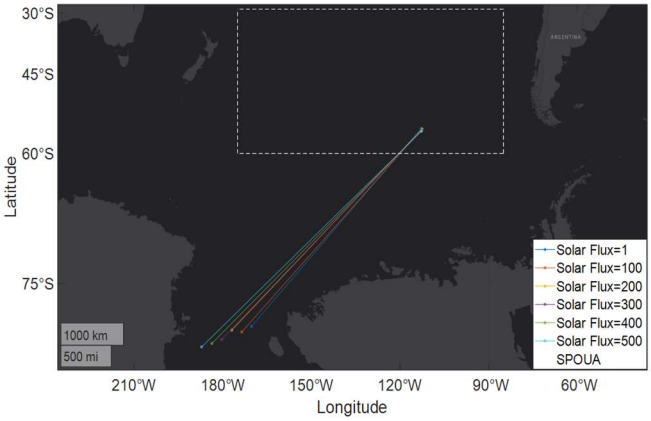

Fig. 11. Solar Flux Sensitivity analysis at 70 km of perigee altitude

6.2.5 Break-up altitude

The comprehension of spacecraft disintegration during re-entry is intricate due to the complex thermo-mechanical conditions they encounter.

Typically, spacecraft disintegrate at altitudes ranging from 84 km to 72 km due to aerodynamic forces surpassing structural limits. The standard breakup altitude is 78 km, as employed in the DRAMA tool. Following disintegration, individual components or fragments gradually lose altitude, experiencing aero heating until they either disintegrate completely or survive to impact the Earth.

In this sensitivity analyses, the results reveal minimal variations as the concept of breakup altitude remains uncertain and challenging to assess, with fragmentation events being a significant source of uncertainty in the re-entry process. The breakup altitude was varied between 60 km and 100 km, revealing that as breakup altitude increases, footprints become longer. However, this effect is mitigated in cases with lower perigee altitudes due to steeper re-entry angles, resulting in more compact footprints.

7. Conclusion

In conclusion, this paper has presented a comprehensive analysis of re-entry trajectories for spacecraft transitioning from Near Rectilinear Halo Orbits (NRHOs) to Low-Earth Orbits (LEOs) within the context of Lunar Orbital Platform-Gateway (LOP-G) missions. Continued research and development in this area will contribute to the success of future space missions, including those involving lunar exploration and beyond.

The study utilized a genetic algorithm (GA) optimization approach to derive optimal trajectory parameters and achieve LEO insertion with minimized ΔV requirements.

Through systematic analyses and the employment of lunar flybys, the study demonstrated that a two-impulse strategy is essential for efficient and feasible LEO insertion from NRHOs. The initial impulse, coupled with lunar influence, substantially reduced the Delta V expenditure required to escape the lunar sphere of influence. This innovative approach highlights the potential for mission cost savings and efficient spacecraft re-entry.

Lastly, it was observed how the initial parameters for the last burn of the re-entry trajectory influence the footprint, underscoring the meticulous planning required for the controlled re-entry phase. This analysis, including off-nominal cases, is essential because the primary objective is to prevent unintentional re-entry into regions beyond the designated South Pacific Ocean Uninhabited Area (SPOUA).

However, further analysis utilizing dynamic models with higher fidelity, potentially extending to n-body problem, is warranted, taking into account lunar eccentricity at epoch from JPL's DE432s ephemerides. For instance, examining five departure dates spanning an entire lunar month allows for an investigation into the departure date's impact on performance in reaching parameterized Low-Earth Orbits (LEOs), considering the epoch-dependent oscillations of Earth-Moon Lagrangian Point 2 (EML2) and the resulting periodic NRHOs. Additionally, for controlled re-entry analysis in the future, a spacecraft-oriented approach could be employed, characterized by detailed modelling of all involved processes and objects, including aero-thermal interactions, thermo-mechanical loads, melting, and deformation. Presently, HTG's SCARAB (Spacecraft Atmospheric Re-Entry and Aerothermal Break-up) tool stands as the sole commercially available spacecraft-oriented modelling software.

List of references

[1] Diane C. Davis, Kenza K. Boudad, Sean M. Phillips, Kathleen C. Howell, “Disposal, deployment, and debris in Near Rectilinear Halo Orbits”, 29th AAS/AIAA Space Flight Mechanics Meeting, January 2019

[2] “Space Innovation IB Docket No. 22-271 Mitigation of Orbital Debris in the New Space Age IB Docket No. 18-313”, FCC-22-74

[3] Luigi Mascolo, “Optimal Escape from Sun-Earth and Earth-Moon L2 with Electric Propulsion”, Doctoral Dissertation in the Graduate School of Politecnico di Torino (ScuDo)

[4] Lee, David E., “White Paper: Gateway Destination Orbit Model: A Continuous 15 Year NRHO Reference Trajectory”, Technical report, National Aeronautics and Space Administration (NASA), 2019, Report/Patent Number JSC-EDAA-TN72594

[5] Pierluigi Righetti, Jose Maria de Juana Gamo, Richard Dyer, “Mission analysis of metop-a end-of-life operations”, EUMETSAT study

[6] AIRBUS, “MetOp-SG Re-entry Analysis”, Ref: MOS-TN-ADST-SYS-1000117622 , Jul 12, 2019

[7] Emily M. Zimovan, Kathleen C. Howell, and Diane C. Davis, “Near rectilinear halo orbits and their application in cis-lunar space”, IAA-AAS-DyCoSS3-125 (2017)

[8] “Debris risk assessment and mitigation analysis (drama) software user manual”, ESA/ESOC Space Debris Office (OPS-SD)

[9] Guzetti, D., Zimovan, E.M., Howell, K.C., Davis, D.C., “Stationkeeping analysis for spacecraft in lunar near rectilinear halo orbits”, AAS-2017-395, AAS/AIAA Spaceflight Mechanics Meeting, San Antonio, Texas (2017)

[10] Zbigniew Michalewicz, “Genetic Algorithms + Data Structures = Evolution Programs”, Third, Reviseted and Extended Edition, Springer, 1996

[11] David E. Goldberg, “Genetic algorithms in search: optimization and machine learning”, Addison-Wesley Longman Publishing Co., 1989

[12] Sourabh Katoch, Sumit Singh Chauhan, Vijay Kumar, “A review on genetic algorithm: past, present, and future”, Springer Science+Business Media, LLC, part of Springer Nature 2020